J|A|C|S
ARTICLES
Published on Web 10/15/2002

Oxysulfide $Sm_2Ti_2S_2O_5$ as a Stable Photocatalyst for Water Oxidation and Reduction under Visible Light Irradiation ($\lambda \leq$ 650 nm)

Akio Ishikawa,[†] Tsuyoshi Takata,[†] Junko N. Kondo,[†] Michikazu Hara,[†] Hisayoshi Kobayashi,[‡] and Kazunari Domen*[,§]

Contribution from the Chemical Resources Laboratory, Tokyo Institute of Technology, Nagatsuta 4259, Midori-ku, Yokohama 226-8503, Japan, Department of Chemistry and Bioscience, Kurashiki University of Science and the Arts, Nishinoura 2640, Tsurajima, Kurashiki 712-8505, Japan, and Core Research for Evolutional Science and Technology, Japan Society and Technology Corporation (CREST, JST), 2-1-13 Higashiueno, Taito-ku, Tokyo 110-0015, Japan

Received May 19, 2002

Abstract: A Ti-based oxysulfide, $Sm_2Ti_2S_2O_5$, was studied as a visible light-driven photocatalyst. Under visible light (440 nm $\leq \lambda \leq$ 650 nm) irradiation, $Sm_2Ti_2S_2O_5$ with a band gap of $\sim$2 eV evolved H_2 or O_2 from aqueous solutions containing a sacrificial electron donor ($Na_2S-Na_2SO_3$ or methanol) or acceptor (Ag^+) without any noticeable degradation. This oxysulfide is, therefore, a stable photocatalyst with strong reduction and oxidation abilities under visible-light irradiation. The electronic band structure of $Sm_2Ti_2S_2O_5$ was calculated using the plane-wave-based density functional theory (DFT) program. It was elucidated that the S3p orbitals constitute the upper part of the valence band and these orbitals make an essential contribution to the small band gap energy. The conduction and valence bands' positions of $Sm_2Ti_2S_2O_5$ were also determined by electrochemical measurements. It indicated that conduction and valence bands were found to have satisfactory potentials for the reduction of H^+ to H_2 and the oxidation of H_2O to O_2 at pH = 8. This is consistent with the results of the photocatalytic reactions.

Introduction

Some Ti^{4+}-, Nb^{5+}-, and Ta^{5+}-based mixed metal oxides, such as $SrTiO_3$[1], $K_2La_2Ti_3O_{10}$[2], $K_4Nb_6O_{17}$[3], and $NaTaO_3$,[4] have been successfully applied for overall water splitting. These oxides, however, are not effective in the visible light region ($\lambda \geq$ 400 nm) because the band gap energies of these materials exceed 3 eV. In these metal oxide photocatalysts, the bottoms of the conduction bands, which consist mainly of the empty transition metal d orbitals, are located at a potential slightly more negative than 0 V versus NHE at pH = 0, and the tops of the valence bands, consisting of O2p orbitals, are at a potential more positive than $\sim$3 V. This situation causes large band gap energies. Some metal sulfides, such as CdS and CdSe, appear to be suitable photocatalysts, since they have energy gaps small enough to absorb visible light and their conduction and valence bands are at sufficient potentials for many redox reactions. These metal chalcogenides, however, are not stable for oxidizing water to form O_2 because the S^{2-} and Se^{2-} anions are more susceptible to oxidation than water; thus, CdS or CdSe are themselves oxidized.[5,6]

In this paper, we describe the photocatalytic reactions and photoelectrochemical properties of the oxysulfide, $Sm_2Ti_2S_2O_5$. $Sm_2Ti_2S_2O_5$ belongs to the *I*4/*mmm* crystallographic group and has the same structure as that of the Ruddlesden−Popper-type layered perovskite oxide, represented by $(AX)(A_{0.5}BX_3)_n$ (A, B = metal cations, X = anions), and the layers are composed of $S-(TiO_2)-O-(TiO_2)-S$ double octahedra.[7,8] It is reported that, under visible light irradiation at $\lambda \leq$ 650 nm, $Sm_2Ti_2S_2O_5$ functions as a photocatalyst for the oxidation of water to O_2 or the reduction of H^+ to H_2 in the presence of a sacrificial electron acceptor (Ag^+) or donor (Na_2S, Na_2SO_3 or methanol), without any noticeable degradation.

Experimental Section

Synthesis of $Sm_2Ti_2S_2O_5$. $Sm_2Ti_2S_2O_5$ samples were obtained by heating a mixture of Sm_2S_3 (99.999%; Soekawa Chemical Co., Ltd.), Sm_2O_3, and TiO_2 (99.95%, 98.5%; Kanto Chemical Co., Inc.) (molar ratio, Sm_2S_3:Sm_2O_3:TiO_2 = 2:1:6)[7,9] in a sealed quartz tube under vacuum at 1273 K. After 4−7 days, the sintered samples were ground

* To whom correspondence should be addressed. E-mail: kdomen@res.titech.ac.jp.
[†] Tokyo Institute of Technology.
[‡] Kurashiki University of Science and the Arts.
[§] CREST, JST.

(1) Domen, K.; Kudo, A.; Ohnishi, T. *J. Catal.* **1986**, *102*, 92.
(2) Takata, T.; Furumi, Y.; Shinohara, K.; Tanaka, A.; Hara, M.; Kondo, J. N.; Domen, K. *Chem. Mater.* **1997**, *9*, 1063.
(3) Kudo, A.; Tanaka, K.; Domen, K.; Maruya, K.; Aika, K.; Onishi, T. *J. Catal.* **1988**, *111*, 67.
(4) Kudo, A.; Kato, H. *Chem. Phys. Lett.* **2000**, *331*, 373.
(5) Ellis, A. B.; Kaiser, S. W.; Bolts, J. M.; Wrighton, M. S. *J. Am. Chem. Soc.* **1977**, *99*, 2839.
(6) Williams, R. *J. Chem. Phys.* **1960**, *32*, 1505.
(7) Boyer-Candalen, C.; Meerschaut, A. *Comp. Rend. Acad. Sci. Série IIC* **1999**, *2*, 93.
(8) Chen, B.-H.; Eichhorn, B.; Wong-Ng, W. *Acta Crystallogr.* **1994**, *C50*, 161.

up and again heated in the vacuum-sealed tube for 7 days. The obtained orange samples were ground into a powder.

Characterization of Catalysts. Characterization of the prepared samples was carried out using X-ray powder diffraction (XRD, Rigaku Geigerflex RAD-B, Cu Kα), scanning electron microscopy (FE-SEM, Hitachi S-4700), energy-dispersive X-ray spectroscopy (EDX, Horiba EMAX-7000), UV−visible diffuse reflectance spectroscopy (UV−vis DR spectra, Jasco V-560), and X-ray photoelectron spectroscopy (XPS, Shimadzu ESCA 3200).

Preparation and Deposition of IrO_2 Colloid. IrO_2 colloid was used as a catalyst for the oxidation of water. The colloid solution was prepared by the hydrolysis of Na_2IrCl_6.[10] The diameters of the IrO_2 particles were estimated to be ∼1−5 nm by transmission electron microscopy (TEM) images of the colloid. While $Sm_2Ti_2S_2O_5$, as prepared, did not adsorb the IrO_2 colloid, the following treatment resulted in the adsorption of the IrO_2 colloid on $Sm_2Ti_2S_2O_5$. A 1.0-g amount of $Sm_2Ti_2S_2O_5$, 1.4×10^{-2} g of $Ca(OH)_2$, and 2 mL of methanol solution were mixed in an agate mortar and ground until dry. The mixture was heated at 573 K under vacuum for 10 min and then washed with distilled water several times to remove excess $Ca(OH)_2$. A 0.3-g amount of $Sm_2Ti_2S_2O_5$ sample loaded with $Ca(OH)_2$ ($Ca(OH)_2/Sm_2Ti_2S_2O_5$) and ∼0.1−12.8 mL of the colloid solution ($IrO_2 \cdot 2H_2O$ ∼0.3−6.0 mg) was added to vigorously stirred distilled water (50 mL). After the solution was stirred for 30 min, the transparent supernatant was decanted and the sample with adsorbed $IrO_2 \cdot 2H_2O$ ($IrO_2-Ca(OH)_2/Sm_2Ti_2S_2O_5$) was rinsed 3 times in distilled water. The sample was dried at 353 K in air. The amount of colloidal IrO_2 adsorbed onto the $Sm_2Ti_2S_2O_5$ was estimated in each case by measuring the absorbance over 500−700 nm of the supernatant rinse solutions. As colloidal IrO_2 has a broad absorption band in the range 500−700 nm,[11] these measurements revealed that 0.3 g of $Sm_2Ti_2S_2O_5$ can adsorb 6 mg of colloidal IrO_2 as the maximum loading.

Photocatalytic Reactions. The reaction was carried out in a Pyrex reaction vessel connected to a closed gas circulation and evacuation system. The photoreduction of H^+ to H_2 and the photooxidation of H_2O to O_2 in the presence of a sacrificial electron donor and acceptor were examined as test photoreactions. H_2 evolution was typically examined in 200 mL of aqueous solution containing 0.20 g of $Sm_2Ti_2S_2O_5$, 1.0 μmol of H_2PtCl_6, and sacrificial electron donors (0.01 M Na_2S−0.01 M Na_2SO_3). The photooxidation of water to O_2 was performed in 200 mL of 0.01 M $AgNO_3$ solution (Ag^+ as sacrificial electron acceptor) containing 0.20 g of $Sm_2Ti_2S_2O_5$ and 0.20 g of La_2O_3 powder. The photooxidation of water decreases the pH of the solution because H^+ is produced with O_2 evolution. In the presence of La_2O_3, the pH of the solution during the photoreaction is buffered at pH = ∼8−9 by the dissolution of La_2O_3 or $La(OH)_3$, a basic metal oxide. To remove air from the reactor, the solution was evacuated several times and then irradiated with a 300-W Xe lamp equipped with cutoff filters. The number of photons reaching the solution was measured with a Si photodiode, and the rate of total incident photons at 440 nm ≤ λ ≤ 650 nm was typically 8.6×10^{21} photons h^{-1}. Quantum efficiency (Φ) values were calculated using the following equation:

$$\Phi\ (\%) = (AR/I) \times 100$$

A, *R*, and *I* represent the coefficients based on the reactions (H_2 evolution = 2, O_2 evolution = 4), the H_2 or O_2 evolution rate (molecules h^{-1}), and the rate of absorption of incident photons, respectively. Here, Φ is the apparent quantum efficiency because we assume that all incident photons are absorbed by the suspension.

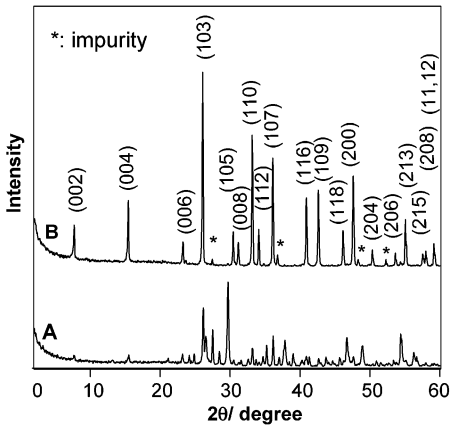

Figure 1. XRD patterns for the samples prepared at 1273 K. Sample A was synthesized by heating the mixture of the starting materials for 4 days. In the case of Sample B, a sintered sample obtained by heating for 1 week was ground and again heated for a further week.

The oxidation of ^{18}O labeled water ($H_2{}^{18}O$) by $Sm_2Ti_2S_2O_5$ under visible light irradiation was carried out in a small Pyrex cell. O_2 evolution was examined in 3 mL of a mixture of $H_2{}^{16}O$ and $H_2{}^{18}O$ ($H_2{}^{16}O/H_2{}^{18}O = 4.2$) containing 0.060 g of $Sm_2Ti_2S_2O_5$, 570 μmol of $AgNO_3$, and 0.06 g of La_2O_3. The time course of gas evolution under visible light irradiation ($\lambda \geq 440$ nm) was analyzed by both gas chromatograph and quadrupole mass spectrometer.

Electrochemical Analysis. The electrochemical properties of $Sm_2Ti_2S_2O_5$ were examined using electrodes fabricated as follows. $Sm_2Ti_2S_2O_5$ powder was pressed into a disk (10 mm diameter, 1 mm thickness). The disk was heated in a vacuum-sealed quartz tube at 1273 K for 1 week. The disk was cut into a square electrode ($1 \times 5 \times 1$ mm^3) after calcination. Metallic indium was sputter-deposited on one side of the electrode, and a Cu wire was attached on the deposited indium film using silver paste. The Cu wire side of the electrode was sealed with epoxy resin to prevent current leakage. The electrode was examined in an electrochemical cell made of Pyrex. A Pt wire and Ag/AgCl electrode were employed as the counter and reference electrodes, and 20 mL of 0.1 M K_2SO_4 was used as the electrolyte. The impedance of the electrochemical cell was measured using a frequency response analyzer (Hz-3000, Hokutodenkou). For photoelectrochemical analysis, the cell was irradiated by a 300-W Xe lamp equipped with a monochromator.

Results and Discussion

XRD Pattern, SEM Image, and UV−vis Spectrum of $Sm_2Ti_2S_2O_5$. Figure 1 shows X-ray diffraction (XRD) patterns for the prepared samples. Sample A was synthesized by heating the mixture of the starting materials for 4 days. In the case of Sample B, a sintered sample obtained by heating for 1 week was ground and again heated for 1 week. Diffraction peaks corresponding to those of $Sm_2Ti_2S_2O_5$[7] appear even in the XRD pattern of Sample A obtained with the short heating time. The intensities of the diffraction peaks increase with increasing heating time, accompanied by a decrease in the impurity phase, as shown in the XRD pattern of Sample B. Energy-dispersive X-ray spectroscopy (EDX) revealed the composition of Sample B to be Sm:Ti:S = 1.0:1.0:0.9 (atomic), an S content slightly lower than the stoichiometric amount. From the scanning electron microscopy (SEM) image of Sample B, shown in Figure 2, the diameters of $Sm_2Ti_2S_2O_5$ particles were estimated to be 2−4 μm. The large size of the $Sm_2Ti_2S_2O_5$ particles is ascribed to the long-duration high-temperature sintering.

(9) Goga, M.; Seshadri, R.; Ksenofontov, V.; Gütlich, P.; Tremel, W. *Chem. Commun.* **1999**, 979.
(10) Harriman, A.; Thomas, J. M.; Millward, G. R. *New J. Chem.* **1987**, *11*, 757.
(11) Harriman, A.; Pickering, I. J.; Thomas, J. M.; Christensen, P. A. *J. Chem. Soc., Faraday Trans. 1* **1988**, *84*, 2795.

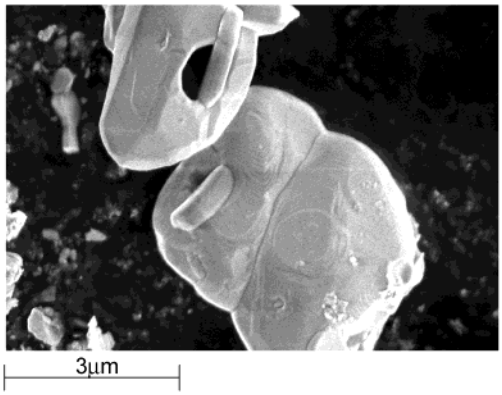

Figure 2. Scanning electron microscopy (SEM) image of $Sm_2Ti_2S_2O_5$ (Sample B).

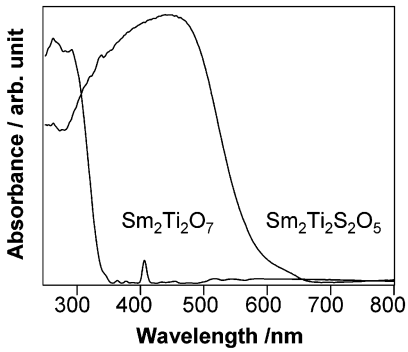

Figure 3. UV−vis diffuse reflectance (UV−vis DR) spectra for $Sm_2Ti_2O_7$ and $Sm_2Ti_2S_2O_5$ (Sample B).

Figure 3 shows UV−vis diffuse reflectance (UV−vis DR) spectra for $Sm_2Ti_2O_7$ and $Sm_2Ti_2S_2O_5$ (Sample B). In the UV−vis spectra, the absorption band edge of $Sm_2Ti_2S_2O_5$ is at 600 nm with a shoulder up to 650 nm, being shifted about 250 nm from that of $Sm_2Ti_2O_7$, and the band gap energy is estimated to be 1.9 or 2.1 eV.

Electronic Structure Calculation. In contrast to the case of the large energy gap of $Sm_2Ti_2O_7$ (∼3.6 eV), the small band gap energy of $Sm_2Ti_2S_2O_5$ is attributable to the incorporation of S^{2-}. Because S3p orbitals have higher potential energies than those of O2p orbitals, the top of the valence band of $Sm_2Ti_2S_2O_5$ may consist predominantly of S3p orbitals, resulting in the small energy gap. To verify this explanation, the band structure of $Sm_2Ti_2S_2O_5$ was calculated using the plane-wave-based density functional theory (DFT) program, CASTEP.[12] The core orbitals were replaced by the ultrasoft core potentials,[13] and the $O2s^2$-$2p^4$, $S3s^23p^4$, $Ti3s^23p^63d^24s^2$, and $Sm5s^25p^64f^66s^2$ electrons were treated explicitly. The kinetic energy cutoff was set to 280 eV. The atomic coordinates of $Sm_2Ti_2S_2O_5$ measured by Boyer−Candalen et al. were used in the DFT calculation.[7] The unit cell includes $(Sm_2Ti_2S_2O_5)_2$ structure, and the total number of valence electrons is 196. Because the Sm4f orbitals have a smaller overlap and lower ionization potential, the SCF convergence is not good. We employed the fractional occupation technique, which allows the withdrawal and accumulation of a small amount of electron density, respectively, in the top of the valence band and the bottom of conduction band.

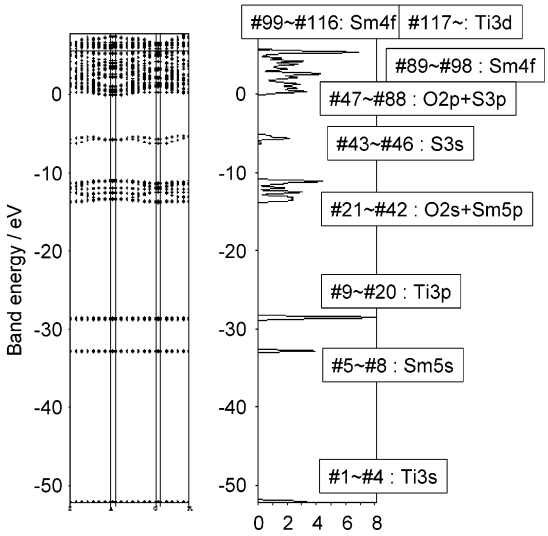

Figure 4. Band dispersion and density of states for $Sm_2Ti_2S_2O_5$.

The calculated band dispersion relation and density of states are shown in Figure 4. In Figure 4, the top of the valence band corresponds to the orbital #98, and the bottom of conduction band, to the orbital #99. The contents of each band are shown in the figure. For example, orbitals from #47 to #88 are composed of O2p and S3p orbitals. The band gap, which is apparently very small, lies between the orbitals #88 and #89. The occupied energy bands obtained in this calculation, in increasing order of energy, are Ti3s, Sm5s, Ti3p, O2s + Sm5p, S3s, O2p + S3p, and Sm4f (part). The unoccupied bands are Sm4f (part) and Ti3d. The valence band is made up of the O2p and S3p hybridized orbitals and the localized Sm4f orbitals. The conduction band consists of the Ti3d and localized Sm4f orbitals. Although the partially filled Sm4f orbitals appear both at the top of valence band and at the bottom of conduction band, their highly localized nature makes them less effective in photoconductivity or photocatalysis and their contribution should, therefore, be ignored when considering photocatalytic and photoelectrochemical phenomena. The apparent electronic structure is like a metal, as shown in Figure 4. However, this is caused by the isolated atom-like Sm4f orbitals, and these orbitals do not contribute to the band gap property. Thus, the band gap is reasonably estimated to be 1.4 eV, as the energy difference between the top of the O2p + S3p band and the bottom of the Ti3d band. This value is just two-thirds of our experimental value (1.9 or 2.1 eV). The major reason for this discrepancy is ascribed to underestimation of the character of the band gap in current DFT.

The DFT calculation indicates that the energy gap of the f−f transition of Sm^{3+} is smaller than the band gap. In contrast, the DRS indicates that the band gap is much smaller than the f−f transition energy, which is mainly observed at ∼400 nm for $Sm_2Ti_2O_7$. The f−f transition energy is evaluated not only from the difference of occupied and vacant 4f orbital energies but also from the electron repulsion term related to the occupied and vacant orbitals. The transition energy for band calculations of solids is usually approximated by only the orbital energy difference if the orbitals are widely extending (i.e., band picture). However, the extension of Sm4f orbitals is rather corelike, and the band picture shown in Figure 4 does not correctly represent the f−f transition energy. The aim of our study is not to evaluate

(12) Payne, M. C.; Teter, M. P.; Allan, D. C.; Arias, T. A.; Joannopoulos, J. D. *Rev. Mod. Phys.* **1992**, *64*, 1045.
(13) Vanderbilt, D. *Phys. Rev.* **1990**, *B41*, 7892.

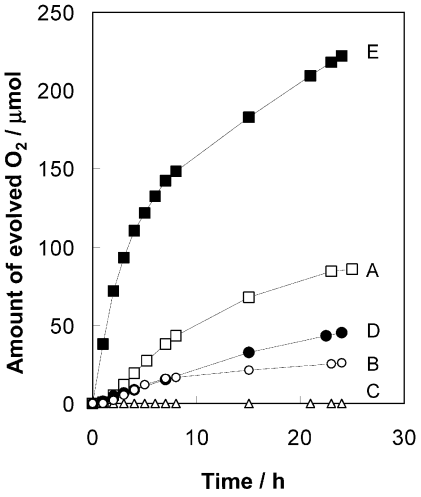

Figure 5. Time courses of O_2 evolution from $Sm_2Ti_2S_2O_5$ and CdS under visible-light irradiation ($\lambda \geq 440$ nm). (A) $Sm_2Ti_2S_2O_5$ (Sample B). (B) $Sm_2Ti_2S_2O_5$ (Sample A). (C) CdS. (D) $Ca(OH)_2/Sm_2Ti_2S_2O_5$. (E) IrO_2 (0.25 wt %)−$Ca(OH)_2/Sm_2Ti_2S_2O_5$, catalyst (0.2 g), 0.01 M $AgNO_3$ solution (200 mL), La_2O_3 (0.2 g).

the f−f transition energy but to estimate the contents of realistic photoexcitation. This is not due to the f−f transition but the transition from the O2p + S3p orbitals to the Ti3d orbitals.

Photocatalytic Reactions of $Sm_2Ti_2S_2O_5$. 1. O_2 Evolution in $AgNO_3$ Solution. Time courses of O_2 evolution on $Sm_2Ti_2S_2O_5$ samples as well as on CdS in $AgNO_3$ solution under visible-light irradiation ($\lambda \geq 440$ nm) are shown in Figure 5. For the as-prepared $Sm_2Ti_2S_2O_5$ sample, O_2 was evolved with irradiation (curves A and B) after a short induction period (~1 h). No reaction took place in the dark. The XRD patterns of $Sm_2Ti_2S_2O_5$ samples before and after the reaction were essentially identical except for the emergence, after the reaction, of a diffraction pattern attributable to metallic Ag. The oxidation of ^{18}O labeled water ($H_2{}^{18}O$) by $Sm_2Ti_2S_2O_5$ under visible light irradiation was performed in an aqueous $AgNO_3$ solution ($H_2{}^{16}O/H_2{}^{18}O = 4.2$, $AgNO_3$ 0.19 M), and it was confirmed that the ratio of $^{16}O/^{18}O$ in evolved O_2 ($^{16}O_2$, $^{16}O^{18}O$, and $^{18}O_2$) was always ~4.2 during reaction (10 h). Apparently, evolved O_2 is derived from water. It was confirmed that O_2 evolution from $Sm_2Ti_2S_2O_5$ depends largely on pH. O_2 evolution was examined in a basic solution (~pH = 8) buffered by La_2O_3, as described above. However, when the reaction was carried out in acidic conditions (pH < ~6), O_2 did not evolve with irradiation. This implies that alkaline conditions are favorable for O_2 evolution on $Sm_2Ti_2S_2O_5$. It is suggested, from the electrochemical analysis shown below, that the valence band of $Sm_2Ti_2S_2O_5$ does not have the satisfactory potential for the oxidation of water to O_2 in acidic conditions with the band gap irradiation. Sample A, which was not completely crystallized in comparison with the case of Sample B, had a slower rate of O_2 evolution than that of Sample B, indicating that the impurity phase lowers the activity of $Sm_2Ti_2S_2O_5$. Sample B was, therefore, used in all subsequent experiments. Despite the impurity phase, the rate of O_2 evolution on Sample A reaches approximately one-half of that of Sample B. This suggests that there still remains a considerable amount of defects, although sample B shows relatively high peak intensities in XRD. The quantum efficiency for O_2 evolution in Sample B was estimated to be 0.2%. For comparison, the time course with CdS under the same experimental conditions is also shown in Figure 5 (curve C). CdS in the $AgNO_3$ solution turned black immediately because of the decomposition of CdS with the formation of Ag_2S, and no O_2 evolution was observed.

It is noteworthy that the O_2 evolution rate increased when we modified the catalyst by the adsorption of IrO_2 colloid, that is, $IrO_2-Ca(OH)_2/Sm_2Ti_2S_2O_5$. Figure 5 also shows time courses of O_2 evolution from $Ca(OH)_2/Sm_2Ti_2S_2O_5$ and IrO_2 (0.25 wt %)−$Ca(OH)_2/Sm_2Ti_2S_2O_5$. While $Ca(OH)_2/Sm_2Ti_2S_2O_5$ had a lower activity for O_2 evolution than that of $Sm_2Ti_2S_2O_5$, the rate of O_2 evolution increased with increasing the amount of adsorbed IrO_2 colloid, reaching a maximum at 0.25 wt %. Further adsorption beyond 0.25 wt % decreased the rate of O_2 evolution. The quantum efficiency at 0.25 wt % adsorption was 1.1%, more than 5 times that of the as-prepared $Sm_2Ti_2S_2O_5$. These results indicate that the IrO_2 colloid functions as an effective O_2 evolution promoter for $Sm_2Ti_2S_2O_5$.

2. $Sm_2Ti_2S_2O_5$ Surface before and after O_2 Evolution under Visible-Light ($\lambda \geq 440$ nm) Irradiation. To evaluate the stability of $Sm_2Ti_2S_2O_5$ during the photooxidation of water in visible light, the surface of the $Sm_2Ti_2S_2O_5$ was examined by XPS. Figure 6 shows the XPS spectra. After reaction for 20 h, the filtrated mixture of $Sm_2Ti_2S_2O_5$ and La_2O_3 was stirred in 100 mL of 1 M HCl solution for 30 min in order to dissolve the La_2O_3, and the $Sm_2Ti_2S_2O_5$ was filtered out for XPS analysis. The total turnover number based on the number of O atoms in $Sm_2Ti_2S_2O_5$ for O_2 evolution (20 h) was 0.1. While the amount of O atoms in $Sm_2Ti_2S_2O_5$ (0.2 g) was 1.9 mmol, that of evolved O_2 in 20 h was 0.10 mmol. Note that the amount of surface O atoms estimated from a BET surface area of 0.59 m^2/g and the (100) face structure of $Sm_2Ti_2S_2O_5$ is 3.8 nmol. Therefore, the turnover number based on the number of surface O atoms was estimated to be $\sim 1.3 \times 10^4$. Even if S^{2-} is oxidized to S^0 species during the reaction, it is known that S^0 species are stable in the HCl solution. There was no significant difference in the binding energies of the $Sm3d_{5/2}$, Ti2p, S2p, and O1s peaks before and after the reaction. In Figure 6A, the intensity of the $Sm3d_{5/2}$ peak after reaction was smaller than that before the reaction, and the O1s peak (Figure 6B) assigned to OH (532.4 eV) became slightly larger after the reaction. The surface atomic ratios of Sm/Ti, S/Ti, and O/Ti are summarized in Table 1. The surface atomic ratios of O/Ti were estimated from O1s peaks at 530 eV. Table 1 shows that the proportions of surface Ti, S, and O did not change during reaction, whereas a considerable amount of Sm disappeared from the surface of the sample after the reaction and HCl treatment. The decrease in surface Sm is not attributed to the photooxidation of water but to the dissolution of Sm^{3+} into the concentrated HCl solution during HCl treatment. As can be seen in Table 1, after a similar HCl treatment, surface Sm also decreased in a sample mixture of $Sm_2Ti_2S_2O_5$ and La_2O_3 powders that did not undergo photoreaction. These XPS and XRD results indicate that the surface and bulk of $Sm_2Ti_2S_2O_5$ are essentially unchanged during the reaction and that $Sm_2Ti_2S_2O_5$ functions as a stable photocatalyst for the oxidation of H_2O to O_2 in $AgNO_3$ solution.

XPS spectra for CdS before and after reaction were also shown in Figure 6D−F. A 0.20-g amount of CdS was irradiated with visible light ($\lambda \geq 440$ nm) for 6 h in an aqueous $AgNO_3$ solution containing La_2O_3 powder, as in the case of $Sm_2Ti_2S_2O_5$. After the reaction, intense peaks of Ag3d appeared and

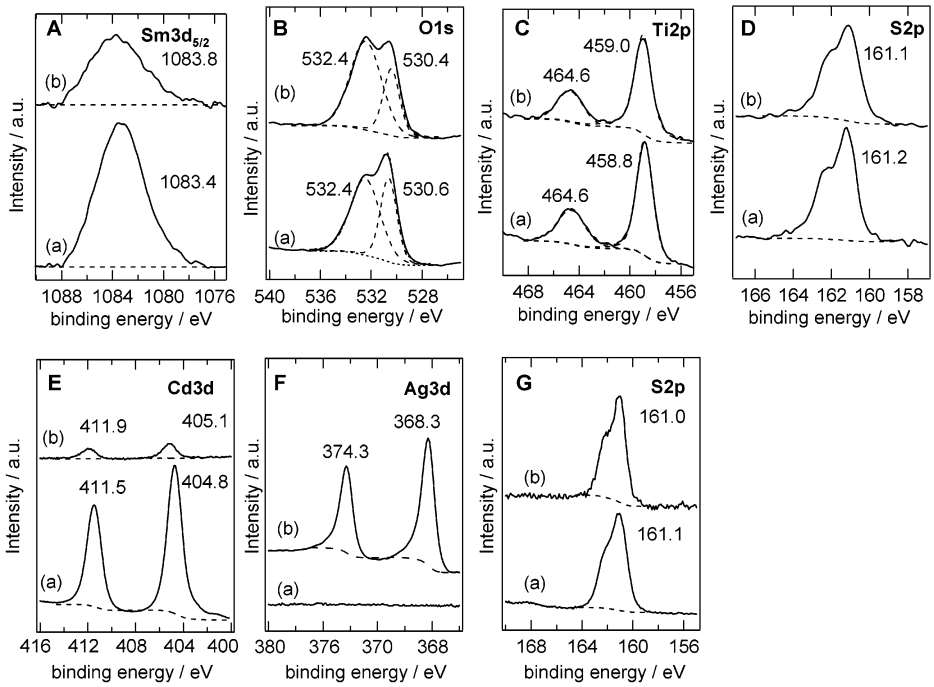

Figure 6. XPS spectra for $Sm3d_{5/2}$ (A), O1s (B), Ti2p (C), and S2p (D) of $Sm_2Ti_2S_2O_5$ before and after O_2 evolution under visible light ($\lambda \geq 440$ nm). The XPS spectra of Cd3d (E), Ag3d (F), and S2p(G) of CdS are also shown. (a) represents before the reaction, and (b), after the reaction.

Table 1. Surface Atomic Ratios of Sm/Ti, S/Ti, and O/Ti of $Sm_2Ti_2S_2O_5$ before (a) and after (b) O_2 Evolution in Visible Light ($\lambda \geq 440$ nm)

sample	Sm/Ti	S/Ti	O/Ti
a	0.7	1.2	3
b[a]	0.23	1.2	2.9
c[b]	0.31	1.2	2.6

[a] After the reaction for 20 h, the filtrated mixture of $Sm_2Ti_2S_2O_5$ and La_2O_3 was stirred in 100 mL of 1 M HCl solution for 30 min in order to dissolve La_2O_3, and $Sm_2Ti_2S_2O_5$ was filtered out for XPS analysis. [b] Sample c was obtained by treating the mixture of $Sm_2Ti_2S_2O_5$ and La_2O_3 powders without photoreaction by HCl solution in a similar manner as that above.

simultaneously Cd3d decreased. The formation of Ag_2S was also confirmed by XRD after the reaction. There was no noticeable difference in XPS spectra and XRD patterns for CdS in dark and under visible-light irradiation for 6 h. These results indicate that, in the presence of Ag^+, CdS surface is transformed to Ag_2S with the dissolution of Cd^{2+} cations. This confirms that CdS is not stable against oxidation by Ag^+ even in a dark condition.

In contrast to the case of CdS, $Sm_2Ti_2S_2O_5$ is stable in dark and under visible-light irradiation, although the valence band partially consists of S3p. $Sm_2Ti_2S_2O_5$ has a layered perovskite-like structure that may be more stable than that of CdS. The formation of $TiSO_5$ octahedra results in the hybridization of S3p and O2p orbitals forming the valence band. It is presumably more than that of pure S3p orbitals.

3. H_2 Evolution in the Presence of Sacrificial Electron Donors. Figure 7 shows the time courses of H_2 evolution on 1.0 wt % Pt−$Sm_2Ti_2S_2O_5$ in the presence of Na_2S−Na_2SO_3 and methanol under visible-light irradiation ($\lambda \geq 440$ nm). The pHs of the aqueous Na_2S−Na_2SO_3 and methanol solutions for H_2 evolution were 13.0 and 5.6, respectively. In the case of the Na_2S−Na_2SO_3 solution, the fastest rate of H_2 evolution was obtained by a Pt loading of 1.0 wt %. In the early stage of the reaction (~3 h), the H_2PtCl_6 added is reduced to Pt^0 as an H_2 evolution promoter on the $Sm_2Ti_2S_2O_5$ surface. After the induction period, H_2 evolves steadily, indicating that excited electrons in the oxysulfide can reduce H^+ to H_2. The quantum efficiency for H_2 evolution at a steady state was 0.1%. XRD and XPS analyses confirmed that H_2 evolution proceeded without any degradation of $Sm_2Ti_2S_2O_5$. This indicates that $Sm_2Ti_2S_2O_5$ also functions as a stable photocatalyst for the reduction of H^+ to H_2 under visible-light irradiation ($\lambda \geq 440$ nm).

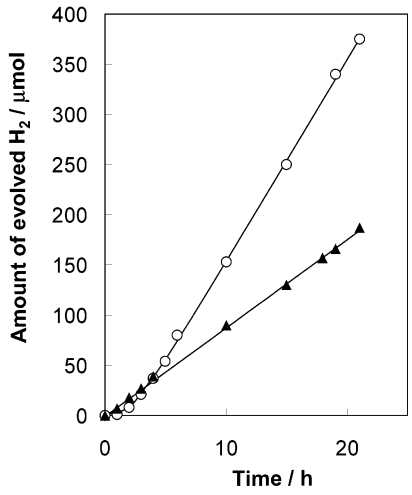

Figure 7. Time courses of H_2 evolution from 1.0 wt % Pt−$Sm_2Ti_2S_2O_5$ under visible-light irradiation ($\lambda \geq 440$ nm). (○) Pt−$Sm_2Ti_2S_2O_5$ (0.2 g), 0.01 M Na_2S, and 0.01 M Na_2SO_3 solution (200 mL); (▲) Pt-deposited $Sm_2Ti_2S_2O_5$ (0.2 g) and 200 mL of methanol solution (distilled water 180 mL, methanol 20 mL).

Figure 7 also displays H_2 evolution in the presence of methanol. The reaction was performed in an aqueous solution (200 mL) containing 0.20 g of the sample loaded with 1.0 wt % Pt and 20 mL of methanol. Pt was loaded by the impregnation method from $[Pt(NH_3)_4]Cl_2$, followed by a reduction in H_2 at

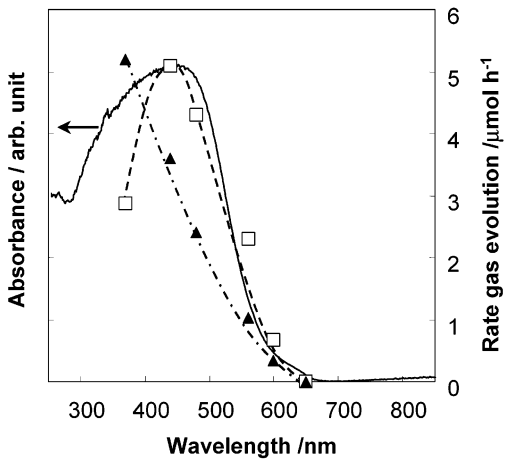

Figure 8. Dependence of the rates of H_2 or O_2 evolution on the cutoff wavelength of incident light and the UV−vis diffuse DR spectrum of $Sm_2Ti_2S_2O_5$. (▲) H_2 evolution from Pt (1.0 wt %)−$Sm_2Ti_2S_2O_5$ (0.2 g)−0.01 M Na_2S and a 0.01 M Na_2SO_3 solution system. (□) O_2 evolution from $Sm_2Ti_2S_2O_5$ (0.2 g)−La_2O_3 (0.2 g)−0.01 M $AgNO_3$ solution system.

573 K. Again, H_2 was evolved steadily, indicating that methanol also works as a sacrificial electron donor on $Sm_2Ti_2S_2O_5$.

Although $Sm_2Ti_2S_2O_5$ and Pt-deposited $Sm_2Ti_2S_2O_5$ were irradiated with visible light in distilled water, no gas evolution was observed. There was no difference between XPS and XRD for the samples before and after the light irradiation. Therefore, it is obvious for photocatalytic overall water splitting in visible light to modify the oxysulfide surface appropriately.

4. Wavelength Dependence. Figure 8 shows the dependence of the steady rate of H_2 evolution and the initial rate of O_2 evolution on the cutoff wavelength of incident light. The filters were used in order to cut off the light with shorter wavelengths than those of the indicated numbers. The UV−vis DR spectrum of $Sm_2Ti_2S_2O_5$ is also shown in the figure to indicate the absorption edge of the oxysulfide. The rates of O_2 evolution were measured using $Sm_2Ti_2S_2O_5$ without IrO_2 colloid. Although both rates decrease with increasing cutoff wavelength due to the reduction in the number of absorbed photons, the evolution of H_2 and O_2 was observed up to ∼600−650 nm, corresponding to the band gap transition of $Sm_2Ti_2S_2O_5$. These photoreactions are, therefore, confirmed to proceed via band gap transition.

Electrochemical Analysis. To study the electrochemical properties of $Sm_2Ti_2S_2O_5$, the electrode was examined under various electrochemical conditions. Figure 9 correlates the current and potential of the $Sm_2Ti_2S_2O_5$ electrode under anodic polarization (pH = 12.7), measured in dark and under intermittent visible-light irradiation ($\lambda \geq 440$ nm). A photocurrent with the oxidation of water is established at ∼>−1.2 V versus Ag/AgCl, indicating that $Sm_2Ti_2S_2O_5$ has an *n*-type semiconductor character and that the flat band potential is ∼−1.2 V.

Figure 10 shows Mott−Schottky (M−S) plots, $1/C^2$ versus E, for the $Sm_2Ti_2S_2O_5$ electrode at pH = 13.2 and 4.1. The M−S plots were obtained at the frequency of 1 kHz. The intersection point of the potential and linear $1/C^2$ potential curves gives a flat band potential, which in this case is approximately −1.4 V versus Ag/AgCl (−1.2 V vs NHE) and almost independent of pH. When the M−S analysis was performed at 1, 2, 5, 10, and 20 kHz, the slopes of the plots increased with increasing frequency. However, no dependence of the intersection points on frequency was observed. The flat band potential

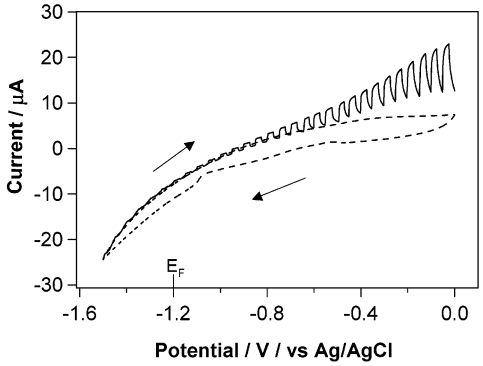

Figure 9. Photocurrent vs potential curve for the $Sm_2Ti_2S_2O_5$ electrode ($\lambda \geq 440$ nm). Counter electrode: Pt. Reference electrode: Ag/AgCl. Electrolyte: 0.1 M K_2SO_4 (20 mL) at pH = 12.7. The solid line is the photoanodic current, and the dashed line is the dark current.

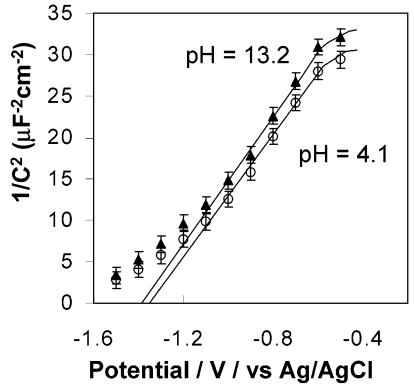

Figure 10. Mott−Schottky plots for the $Sm_2Ti_2S_2O_5$ electrode. (▲) pH = 13.2; (○) pH = 4.1. Counter electrode: Pt. Reference electrode: Ag/AgCl. Electrolyte: 0.1 M K_2SO_4 (20 mL). Frequency: 1 kHz.

of the $Sm_2Ti_2S_2O_5$ electrode was, therefore, estimated to be ∼−1.4 V versus Ag/AgCl (−1.2 V versus NHE) which is independent of pH. This is consistent with the photocurrent−potential curve in Figure 9: the photocurrent is observed at ∼−1.2 V versus Ag/AgCl. The dependence of the slopes of the linear M−S plots on used frequency can be attributed to the polycrystalline $Sm_2Ti_2S_2O_5$ electrode. In the case of polycrystalline electrodes, the slopes of the linear M−S plots depend on the frequency in M−S analysis because of various surface states.

From the measurement of the relative permittivity of the oxysulfide, the difference between the bottom of conduction band and the Fermi level was estimated to be ∼0−0.1 eV.[14] It

(14) The slope of M−S plots ($(1/C^2)$/V) is expressed by the following equation:[15] $(1/C^2)/V = 2/(q\epsilon_r\epsilon_0 N_D)$, where q, ϵ_r, ϵ_0, and N_D represent the elementary electric charge (1.60×10^{-19} C), relative permittivity, vacuum permittivity (8.85×10^{-14} F cm^{-1}), and concentration of donor impurities in bulk, respectively. ϵ_r was estimated to be 23 by an impedance analyzer. Because $(1/C^2)$/V increased from 2.5×10^{13} to 4.0×10^{13} cm^4 V^{-1} with increasing measurement frequency (1∼20 kHz) as mentioned above, N_D was estimated to be $\sim 1.5 \times 10^{17}$−2.5×10^{17} cm^{-3}. The difference between the conduction band and Fermi levels ($\Delta E = E_C - E_F$) is given by the following equation: $n_0 = Nc \exp(\Delta E/kT)$, $Nc = 2.5 \times 10^{19}(m_C/m_0)^{3/2}(T/300)^{3/2}$. As a first approximation, n_0 (total concentration of donor impurities in bulk and on surface) is equal to N_D. m_C and m_0 are the effective mass of the electron in the conduction band and the effective mass of the electron (9.11×10^{31} kg), respectively. In the band structure analysis for metal oxides such as TiO_2 ($\epsilon_r = 173$, $N_D = 3 \times 10^{20}$ cm^{-3}), SnO_2 ($\epsilon_r = 23.4$, $N_D = 3 \times 10^{18}$ cm^{-3}), $KTaO_3$ ($\epsilon_r = 243$, $N_D = 1 \times 10^{18}$ cm^{-3}), and $KTa_{0.77}Nb_{0.23}O_3$ ($\epsilon_r = 243$, $N_D = 2 \times 10^{17}$ cm^{-3}), m_C/m_0 can be approximated as 1.0. In the case of GaN ($\epsilon_r = 7$, $N_D = 6 \times 10^{17}$ cm^{-3}), m_C/m_0 has been estimated to be 0.2. It is difficult to determine a correct m_C of $Sm_2Ti_2S_2O_5$ because prepared $Sm_2Ti_2S_2O_5$ is polycrystal. However, assuming that m_C/m_0 is 0.2∼1.0 in $Sm_2Ti_2S_2O_5$ which has high electron density and low resistance, we can estimate ΔE to be ∼0−0.1 eV.

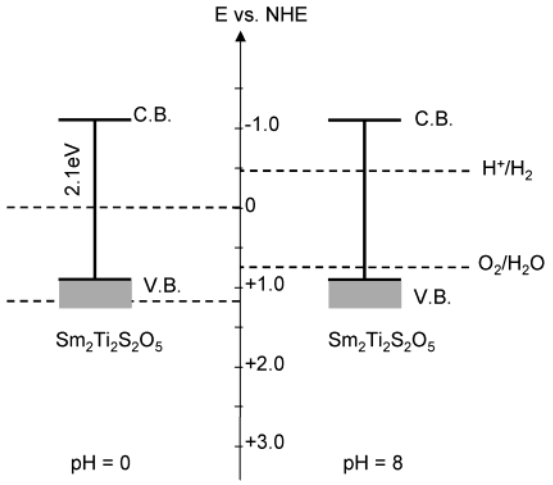

Figure 11. Estimated band positions of $Sm_2Ti_2S_2O_5$ at pH = 0 and 8.

is generally known that the bottom of the conduction bands in many *n*-type semiconductors is more negative by ~ -0.1 V than the flat band potential.[16,17] The estimated band structure of $Sm_2Ti_2S_2O_5$ is illustrated in Figure 11. The conduction and valence bands have enough potentials for the reduction of H^+ to H_2 and the oxidation of water to O_2 at pH = 8 with the band gap irradiation, and this is consistent with the results of the photocatalytic reactions.

Interestingly, the flat band potential of $Sm_2Ti_2S_2O_5$ is almost independent of pH. In metal oxide photocatalysts such as TiO_2, the flat band potential shifts to more negative potentials with increasing pH because of the dissociation of surface hydroxyl groups. As shown in the XPS spectra, $Sm_2Ti_2S_2O_5$ has surface hydroxyl groups, while the flat band potential is unchanged for pH. A possible explanation for that is the small acid dissociation constant of hydroxyl groups on $Sm_2Ti_2S_2O_5$. S in $S-(TiO_2)-O-(TiO_2)-S$ or Sm might give rise to this feature of the hydroxyl groups.

In the case of $Sm_2Ti_2S_2O_5$, the difference between the oxidation potential of water and the valence band level is small, so that the oxidation of water is not efficient. Such an appropriate surface modification as the deposition of an O_2 evolution catalyst or synthesis of oxysulfides with valence band levels suitable for the oxidation of water might result in the efficient oxidation of water under visible-light irradiation. These possibilities are currently under investigation.

Conclusion

$Sm_2Ti_2S_2O_5$, a Ti^{4+}-based oxysulfide, was confirmed to be a stable visible light-driven photocatalyst for the oxidation of water to O_2 or the reduction of H^+ to H_2 without the oxidation of S^{2-} or the decomposition of the structure. The bottom of the conduction band and the top of the valence band are sufficient for the reduction of H^+ and the oxidation of water, respectively. As such, this oxysulfide performs as a stable photocatalyst for H_2 or O_2 evolution from an aqueous solution containing a sacrificial electron donor or acceptor under visible light ($\lambda \leq$ 650 nm).

The deposition of an IrO_2 colloid on $Sm_2Ti_2S_2O_5$ as an O_2 evolution promoter enhanced the photooxidation activity 5-fold, demonstrating that such a surface modification can improve the photocatalytic activity of $Sm_2Ti_2S_2O_5$.

Acknowledgment. This work was supported under the Core Research for Evolutional Science and Technology (CREST) program of the Japan Science and Technology Co. (JST).

JA0269643

(15) Bolts, J. M.; Wrighton, M. S. *J. Phy. Chem.* **1976**, *80*, 2641.
(16) Matsumoto, Y. *J. Solid State Chem.* **1996**, *126*, 227.
(17) Matsumoto, Y.; Omae, K.; Watanabe, I.; Sato, E. *J. Electrochem. Soc.* **1986**, *133*, 711.